Optical interferometric technique for deformation analysis

S. Yoshida, Dr. Muchiar, I. Muhamad, R. Widiastuti, A Kusnowo

Optical interferometric technique for deformation analysis

Sanichiro Yoshida*, Muchiar, I. Muhamad, R. Widiastuti and A. Kusnowo

Research and development Center for Applied Physics, Indonesian Institute of Sciences, PUSPIPTEK, Serpong, Tangerang 15310, Indonesia

yoshida@phys.ufl.edu

Abstract: We have developed a unique optical interferometric technique for deformation analysis and have applied it to tensile analyses of aluminum based samples. Using a recent theory of plastic deformation, this technique is capable of diagnosing whether the sample is close to a fracture and where the fracture will occur. It is also capable of diagnosing the current degree of stress concentration being developed in the sample. The theoretical basis of this method and some experimental results are presented.

OCIS codes: (120.6160) Speckle interferometry; (120.4290) Nondestructive testing

*Present address: *University of Florida, Department of Physics P.O. Box 118440, Gainesville, FL 32611-8440*

References and links

1. V. E. Panin, *Physical mesomechanics and computer-aided design of materials*, vol.1, (Nauka, Nobisobirsk, 1995) (Russian).
2. O. J. Løkberg, "Recent Developments in Video Speckle Interferometry," in *Speckle Metrology*, R. S. Sirohi, ed. Optical Engineering, Vol. 38, (Marcel Dekker, New York, Basel, Hong Kong, 1993) pp. 157-194.
3. Sanichiro Yoshida, Suprapedi, Rini Widiastuti, Marincan Pardede, Septriyanti Hutagalung, Julinda S. Marpaung, A. Faizal Muhardy and Anung Kusnowo, "Direct Observation of Developed Plastic Deformation and Its application to Nondestructive Testing," Jpn. J. Appl. Phys. **35**, L854-L857 (1996).
4. S. Yoshida, Suprapedi, R. Widiastuti, Marincan, Seprtiyanti, Julinda, A. Faisal and A. Kusnowo, "A novel, optical nondestructive deformation analyzer based on electronic speckle-pattern interferometry and a new plastic deformation theory," in *Abstract Proceedings of the VIII International Congress on Experimental Mechanics and Experimental/Numerical Mechanics in Electronic Packaging*, (Society for Experimental Mechanics, Nashville, Tennessee, June 10 - 13, 1996) pp. 168-169.
5. S. Yoshida, Muhiar, I. Muhamad, R. Widiastuti, B. Siahaan, M. Pardede and A. Kusnowo, "New optical interferometric technique for stress analysis" in *Proc., 3rd International conference on modern practice in stress and vibration analysis*, M. D. Gilchrist ed, (A. A. Balkema, Dublin, Ireland, September 3-5, 1997) pp. 361-363.
6. S. Yoshida, I. Muhamad, M. Pardede, R. Widiastuti, Muchiar, B. Siahaan and A. Kusnowo, "Optical interferometry applied to analyze deformation and fracture of aluminum alloys," Theor. and Appl. Fracture Mechanics **27**, 85-98 (1997).
7. V. E. Panin and V. S. Pleshanov, "Banded structure on meso- and macro-scale level in elastic polycrystal," in *Physical Mesomechanics and Computer-aided Design of Materials*, V. E. Panin, ed. Vol.1 (Nauka, Novosibirsk, 1995), pp. 241-248 (Russian).
8. S. Toyooka, private communication, July, 1997.
9. V. E. Panin, "Physical basis of mesomechanics of plastic deformation and fracture of solid-state materials," in *Physical Mesomechanics and Computer-aided Design of Materials*, V. E. Panin, ed. Vol.1, (Nauka, Novosibirsk, 1995), pp. 7-49 (Russian).
10. V. E. Panin, "Physical mesomechanics of plastic deformation and experimental results obtained by optical methods," Oyobuturi **64**, 888-894 (1995) (English).
11. V. P. V. Makarov, "Dynamic theory of plasticity and fracture in structurally non-homogeneous media," in *Physical Mesomechanics and Computer-aided Design of Materials*, V. E. Panin, ed. Vol.1, (Nauka, Novosibirsk, 1995), pp. 78-101 (Russian).
12. See for example, R. S. Sirohi, "Speckle methods in experimental mechanics," in *Speckle Metrology*, R. S. Sirohi, ed. Optical Engineering Vol. 38, (Marcel Dekker, New York, Basel, Hong Kong, 1993) p. 125
13. V. E. Panin, "Contemporary problems in physics of plasticity and durability of solid-state media," *Structure level of plastic deformation and fracture*, V. E. Panin, ed. (Nauka, Nobisobirsk 1990) p. 8 (Russian).

1. Introduction

In most of the conventional techniques of nondestructive testing (NDT) of solid-state materials, it is a usual practice to inspect the object for a crack and monitor its development. Thus the existence of a crack is prerequisite. This type of approach is reliable to predict the location and timing of a fracture once the crack responsible for the fracture is found, but it does not provide any clue of fracture until a crack is found. In addition, it is not easy to find a crack in its early stage, and in some cases the crack is too large when it is found. For these reasons, we are interested in a technique that enables us to diagnose the current degree of deformation, to predict how the deformation progresses from that point of the time, and to locate where the material eventually fractures without relying on the existence of a crack. Our idea is basically to monitor deformation by an optical interferometric technique, diagnose the current mechanical state of the material and update the diagnosis at every time step so that the fracture may be predicted as an early state as possible.

For such an approach, two features are important; first, it is essential to use a theory of deformation that describes all the stages of deformation inclusively so that the evolution of deformation can be diagnosed properly at each stage in connection with the fracture. Recently, Panin et. al. [1] have developed a theory of plastic deformation and fracture called mesomechanics that meets this requirement. Using a gauge theoretical approach, mesomechanics is capable of describing all the stages of plastic deformation, including the fracture as its final stage, in the same theoretical system. It is also important to note that mesomechanics is applicable universally to solid-state materials that have an inner-structure. The other feature important for our approach is the capability of acquiring data on a real time basis with the minimum amount of computation so that the diagnosis may be updated as the deformation evolves with as a small interval as possible. For this purpose, we employ the electronic speckle pattern interferometry (ESPI) [2] for image acquisition. The advantages of our particular ESPI arrangement are: it does not require rearrangement of the optics and therefore suitable for real-time data acquisition, it is robust against ambient vibration and therefore is realistic for field uses, and the amount of computation is small.

With the above-mentioned features in mind, we have carried out a number of experiments. We have found that a specific optical band pattern observed in an interferometric fringe system can be used for the above-mentioned type of diagnosis. Since this optical band pattern appeared conspicuously white on our black-and-white monitor when we discovered it, we call it the white band (WB) [3]. By monitoring the shape and motion of a WB, it is possible to diagnose whether the material is about to fracture and predict where the fracture will occur. It is also possible to judge if the material has initial stress concentration [4]. The latter can be used, for example, to evaluate the residual stress in the heat affected zone of a weld [5]. Using mesomechanics, we have explained the WB as representing a material scientific band structure [6] called the mesoband [7]. According to mesomechanics, the mesoband represents strain localization responsible for the generation of a crack. This situation has generated the possibility of using the present method as a unique optical NDT that can be widely applied to a various types of materials. The aim of this paper is to introduce this method and demonstrate its operation using results of our recent tensile analyses of aluminum alloys. Toyooka et all [8**]** have observed the same phenomenon in stainless steels.

2. Theoretical basis

2.1 Mesomechanics and mesoband

According to mesomechanics [9, 10], the plastic deformation is the loss of shear stability. It is a relaxation process that develops through a hierarchy of scale levels called micro-, meso- and

macro-level. In each level, stress concentration caused by defects relaxes through interaction between tanslational and rotational modes of deformation. Intuitively, this interaction may be understood as follows. If a slip (translational-mode deformation) occurs in a specimen under stress, it causes part of the material (deformation structural element, DSE) to rotate (rotational-mode deformation). This material rotation, called the primary rotation, induces a secondary rotation of the opposite direction in the neighboring DSE so that the total angular momentum may be conserved. This secondary rotation in turn causes a new slip called the secondary slip in that DSE. In this way, a translational flow of a lower level induces a rotation of a higher level, causing the plastic deformation to develop its scale level. Because of such interaction between the translational and rotational modes, the plastic deformation is basically a spatial-temporal wave phenomenon and the displacement vector field is vortical (See Fig1and Fig3).

In each level of deformation, a band structure appears at the boundary of adjacent vortexes that have mutually opposite directions of rotation [7]. In dissipation theoretical terms, the formation of a band is associated with relaxation of the system. Because of these opposite rotations, a bend moment operates along the band structure and strain tends to be localized where the band appears. As the deformation evolves, neighboring vortexes are integrated to a vortex of a larger scale. Thus the scale of the vortexes grows whereas the number of vortexes decreases. During this process, the level of the band structure grows, and consequently, a larger bend moment operates at the band. This makes the material tend to be discontinuous at the band, and this can cause a crack. If the degree of deformation is not critically high, however, the strain localization possibly fades as the stress concentration relaxes, and the material recovers from the discontinuous situation [10]. The vortexes at both sides of the band disappear and a similar band is formed at a different location where the same process occurs. In other words, the band is dynamic. This situation is illustrated in Fig.1 where a set of displacement velocity fields calculated by P. V. Makarov show (a) a pair of developed vortexes, (b) the material is observed to be discontinuous at the boundary of these vortexes, and (c) some time later the vortexes disappear so does the discontinuity. The band structure appears at the boundary of such a pair of vortexes.

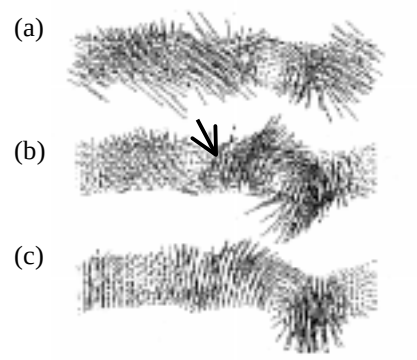

FIG.1 Vortexes observed in a set of calculated displacement velocity fields (ref.11). (a) A pair of vortexes appear; (b) the material becomes discontinuous at the boundary region (see arrow); (c) some time later the vortexes disappear and the material recovers from the discontinuous situation.

When the deformation enters the final stage, all the vortexes are integrated into two highly developed vortexes having mutually opposite direction of rotation, and a large-scale band structure called the mesoband appears along the boundary of the two vortexes (see Fig3). In this condition, the strain is mostly concentrated along the mesoband, and this situation is called intensive strain localization. (Imagine a sample whose upper and lower parts are respectively rotated in the opposite directions.) In this stage, the material becomes

discontinuous around the mesoband and does not recover, and this causes the generation of a crack. If this happens, the stress relaxation is sustained by further enhancing the discontinuity (intensive strain localization) and the material can fracture at any moment. The band at this stage is sometimes called the macroband (there is no clear boundary between the usage of the words mesoband and macroband. In this paper we use the word mesoband to mean a band of this stage inclusively).

2.2 Electronic speckle-pattern interferometry and white band (WB)

The WB is observed in a fringe pattern formed in the subtraction mode of in-plane sensitive ESPI. The principle of the fringe formation can be found in a number of literatures [12]. In short, a fringe pattern is generated by the follow mechanism. Imagine an object illuminated by two coherent beams from a common laser source with the same angle of incidence α (Fig.2). The total intensity of an image of this object can be written as

$$I_{bf}(x, y)=I_1 + I_2 + 2(I_1 I_2)^{1/2} \cos(\theta(x,y)) \quad (1)$$

where I_1 and I_2 are the average intensities (dc term) of the respective beams, $\theta(x,y)$ is the phase difference between the two speckles formed by the respective beams at a point P(x, y) on the object and the subscript bf indicates that I_{bf} is the image taken before the displacement of interest occurs. If point P displaces in a direction parallel to the x axis in such a way that the optical path for the first beam may be increased by ϕ (x,y)/2, the optical path for the other beam will be decreased by $\phi(x,y)/2$. Thus the total change of the phase difference between the two speckles will be $\phi(x,y)$ and the resultant intensity can be written as

$$I_{af}(x, y)=I_1 + I_2 + 2(I_1 I_2)^{1/2} \cos(\theta(x,y) + \phi(x,y)), \quad (2)$$

where the subscript af indicates that I_{af} is the image taken after the displacement of interest occurs. Then if I_{af} is subtracted from I_{bf}, the result is

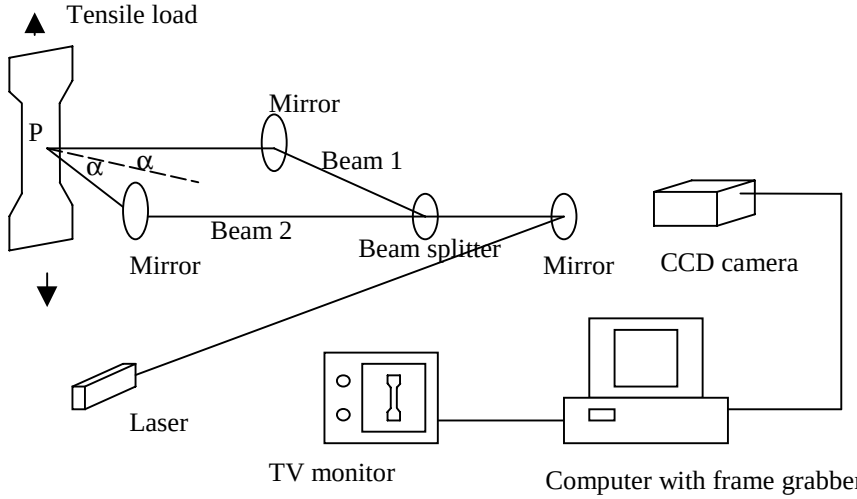

FIG.2 Experimental setup. Two arms of interferometers have the same angle of incidence α For clarity only the horizontal interferometer is shown.

$$\Delta I(x, y)= 2(I_1 I_2)^{1/2} \sin(\theta(x,y) + \phi(x,y)/2) \sin(\phi(x,y)/2). \quad (3)$$

Equation (3) indicates that if the phase change $\phi(x,y)$ is a multiple of 2π, $\Delta I(x, y)$ becomes zero no matter what the initial phase difference $\theta(x, y)$ may be. If the displacement is a smooth function of x, as is usually the case of elastic deformation, $\phi(x,y)$ varies from a certain value to a different value through periods of 2π over a given distance on the object. This causes $\Delta I(x, y)$ to vary from zero to a peak value periodically, where $\Delta I(x, y)$ becomes zero when $\phi(x,y)=2N\pi$, i.e., if $I_{bf}(x, y)$ and $I_{af}(x, y)$ correlate with each other completely, and $\Delta I(x, y)$ takes a peak value when $\phi(x,y)=(2N+1)\pi$ with N being an integer , i.e., $I_{bf}(x, y)$ and $I_{af}(x, y)$ do not correlate with each other. Therefore, the map of $\Delta I(x, y)$ shows a system of fringes, where the dark fringe corresponds to $\phi(x,y)=2N\pi$, the bright fringe corresponds to $\phi(x,y)=(2N+1)\pi$, and the intermediate intensity (gray level) corresponds to an intermediate value of $\phi(x,y)$. Note that the spatial variation of $\Delta I(x, y)$ is sinusoidal provided that the spatial variation of $\phi(x,y)$ is moderate.

In a deformation analysis, the above procedure is taken continuously with a given interval. Fig.2 illustrates an experimental arrangement in which we observe the WB. We apply a tensile load to the sample object by a universal-test-machine at a cross-head speed ranging from 0.35 to10 mm/min. The optical setup is a usual in-plane sensitive, two-dimensional, double-beam ESPI arrangement [2], where a pair of dual-beam interferometers sensitive to the vertical and horizontal displacement of the object, respectively, are arranged.(In Fig.2 only the horizontal interferometer is shown to avoid complexity. The vertical interferometer is identical to the horizontal interferometer except that it is rotated by 90 deg around an axis normal to the object.) At a time step t_i, we take $I_{bf}(i)$ by a CCD (charge coupled device) camera and transfer the output to a computer memory through a frame grabber. After a preset deformation duration Δt, we take $I_{af}(i)$. Then the computer makes subtraction between $I_{bf}(i)$ and $I_{af}(i)$ and the resultant fringe pattern is displayed on the TV monitor. This procedure is repeated with a preset data acquisition interval of ΔT until the sample fractures. We usually use Δt=2 - 6 s and ΔT=10 - 15 s. In parallel to this image acquisition, we record the elongation of the object together with the load by an x-y plotter.

The WB is observed in a fringe pattern as a bright band that can be differentiated from the bright peaks of surrounding fringes by its sharper edges and uniform intensity. As is the case of the bright peak of a usual fringe system, the WB is formed by decorrelation between I_{bf} and I_{af} when a band-shaped block of the material displaces as a whole. Since the entire region of this block displaces by the same amount, it corresponds to a common value of phase change ϕ. Therefore, the intensity is uniform unlike the case of the bright peak of a usual fringe system where the intensity varies sinusoidally depending on the spatial function $\phi(x, y)$ (eq. (3)). The brightness of a WB is determined by the value of this spatially constant ϕ through $\sin(\phi/2)$, i.e., as ϕ gets closer to $(2N+1)\pi$, the brightness increases and, to the contrary, if ϕ happens to be $2N\pi$, the brightness becomes zero. In fact we occasionally observed such a completely dark WB (should be called a black band?) in our experiments.

From the material scientific viewpoint, the WB is interpreted as the band-shaped displacement associated with the formation of a mesoband [7]. According to mesomechanics, a mesoband is formed at the boundary of two meso-scale vortexes having opposite rotations when a meso-scale defect propagates as a process of stress relaxation [9]. This indicates that if the WB represents a mesoband it should be observed at the boundary of such a pair of vortexes and that its formation should be accompanied by stress relaxation. We have confirmed that these are the cases in our previous experiments. Fig.3 illustrates our observation that a pair of highly developed vortexes having mutually opposite directions of rotation appear at both sides of a region along which a WB is observed immediately afterwards [6]. We have also observed that the appearance of the first WB coincides with the initiation of zigzag characteristic observed in the stress-strain curve (see Fig.5 and Fig.8

below) [6]. Mesomechanics explains that this zigzag characteristic is initiated when the stress reaches the critical level in which the carrier of plastic deformation starts to move and finishes when the stress reaches the minimum level to maintain this motion of the deformation carrier [13]. Thus it can be said that the displacement responsible for the formation of a WB is caused by this motion of the deformation carrier.

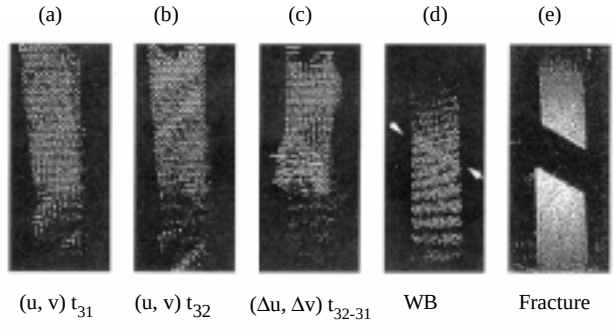

Fig.3 WB and a pair of vortexes observed at both sides of a WB (ref.6). (a) and (b) show displacement vector fields observed at time steps 31 and 32, respectively. (c) shows the change of these displacement fields. A pair of vortexes rotating clockwise (upper) and counterclockwise are observed. (d) shows a stationary WB that appears shortly after at the boundary of the vortexes. (e) The sample eventually fractures along this WB.

2.3 Diagnosis of deformation by WB

As mentioned in 2.1, a mesoband is formed when and where strain localization occurs, and it disappears if the strain localization fades out; if the strain localization is intensive, the mesoband stays at the same location making the material discontinuous, and this leads to the formation of a crack and eventually a fracture. This and the fact that the WB represents the mesoband indicate that this transition of a mesoband should be manifested as a temporal change of the corresponding WB. Fig.4 shows an example of such a change of a WB observed in a tensile-loaded aluminum alloy sample. This sample is free of initial stress concentration and this is one of the cases where the transition of the stress condition is manifested as the change in the WB's feature most clearly. When the material is free of initial stress concentration, the WB normally begins to appear as soon as the deformation enters the plastic region. In an early stage when the stress concentration is still low, the WB appears to be relatively broad and usually runs in the direction of the maximum shear stress (45 deg to the tensile axis). This indicates that the displacement due to the associated stress relaxation is in the direction of the maximum shear stress and the strain is localized in a relatively broad region. Often, more than one WB are observed simultaneously (Fig4a), and they disappear after a while and similar band reappear at different locations of the object. These manifest the above-mentioned phenomenon that strain localization occurring under a not critically high degree of deformation fades out as the stress concentration relaxes and similar strain localization is generated at a different location of the object. WBs showing these features indicate that intensive strain localization has not developed yet, and therefore the material is not yet in the stage of fracture. Since the WB looks like moving around the object, we say that the WB is dynamic and therefore the material will not fracture yet.

As the deformation progresses, the WB tends to be narrower (Fig.4b), and does not necessarily run in the direction of the maximum shear stress. This indicates that the strain is localized in a narrower region. In this stage, normally one WB is observed at a time and it tends to be stationary. When the deformation further progresses, the WB becomes completely stationary and runs in the direction of the line along which the material eventually fractures

(Fig.4c). Apparently this corresponds to the above-mentioned stationary mesoband representing intensive strain localization that is responsible for the fracture. We say that the WB becomes stationary and the material can fracture at any moment. Very importantly, the fracture always occurs at the location where the WB becomes stationary (Fig. 4d). Fig.4e shows the time historical change of the location of the WB on the object surface, where the location is expressed in pixel number of the image (hereafter we call this change of WB's location the dynamic characteristics of a WB). In Fig.4f, we display a series of WB images observed in a similar sample to show how this transition from dynamic WBs to stationary WBs appear on a TV monitor.

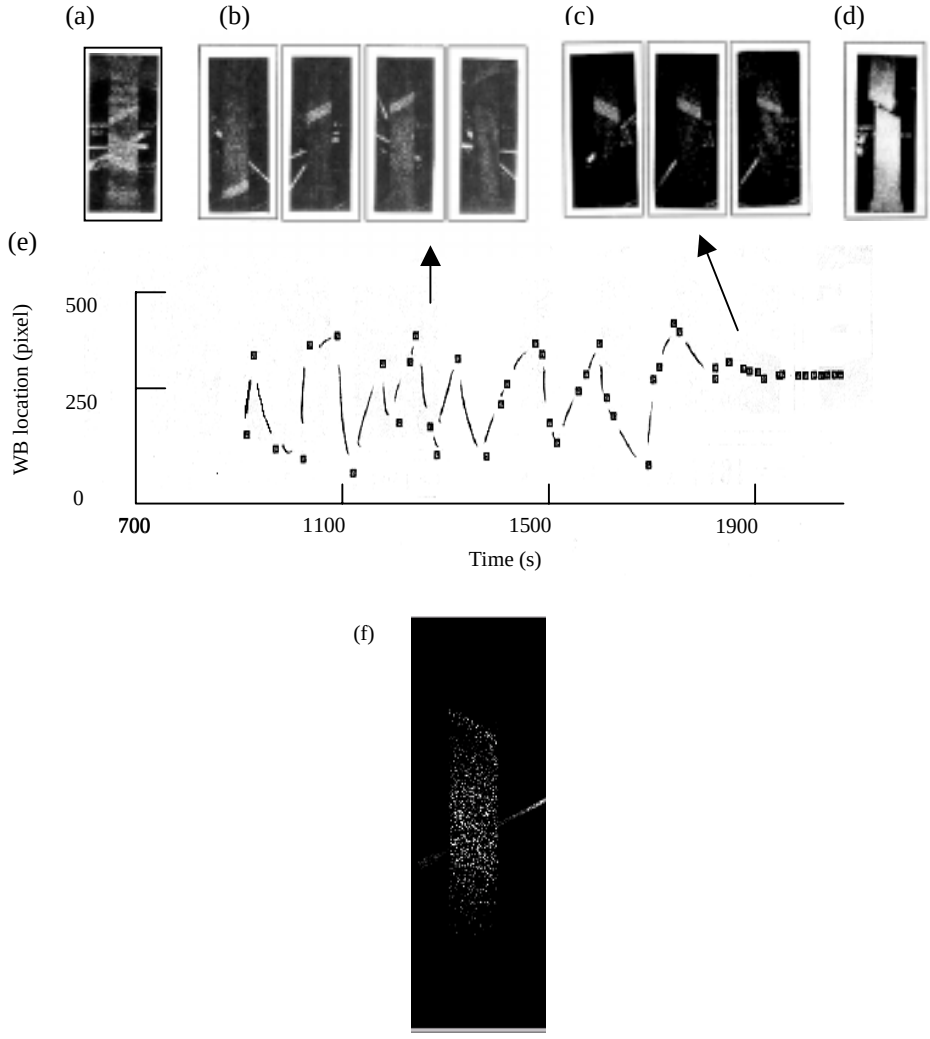

Fig.4 Typical WB observed in a sample free of initial stress concentration; (a) multiple WBs observed in an early stage; (b) dynamic WBs in the intermediate stage; (c) stationary WBs in the final stage; (d) the fracture; (e) the time historical change of WB location (dynamic characteristics of WB); and (f) transition from dynamic to stationary WBs as observed on a TV monitor (animated images). The white lines seen in the background of the images are part of the hands of a clock placed behind the sample.

From what described above, the basic diagnostic criteria can be concluded as follows:

(1) If a WB does not appear, there is no meso-scale strain localization in the material.
(2) If a WB appears and is dynamic, there is strain localization of the meso-scale, but it has not reached the intensive level and therefore the material is not in the stage of fracture.
(3) If the WB becomes stationary, the strain localization is on the intensive level and the material can fracture at any moment at the location where the WB becomes stationary.

3.WB under various stress conditions

Being associated with strain localization, the characteristics of the WB are strongly related to stress concentration. Therefore, if the material has initial stress concentration, the feature of the WB varies dramatically, depending on the degree of the stress concentration. Here the word initial is used to mean prior to the application of a tensile load. In this section we discuss how initial stress concentration of various degrees affects the characteristics of the WB. We gave initial stress concentration to samples by welding them with a carbon dioxide laser under different welding conditions. Voids generated in the heat affected zone cause stress concentration.

3.1 Samples

All the samples have a common size of 150 mm in effective length, 25 mm wide and 2 mm thick. The aluminum alloys tested are A5052H112, A5052H32 and AA6063. The first two are standard materials with specification guaranteed by the manufactures. They have the same chemical composition and both are work-hardened after the casting process. The only difference between them is that A5052H32 is given stabilization treatment after the hardening treatment while A5052H112 is not. The sample based on AA6063 is a low grade material whose specification is not guaranteed except that its composition is known to be AA6063. We welded some of the A5052H32 samples. Table1 summarizes the conditions of these samples:

Table 1. Samples

sample ID	material	stabilization	welding condition
(1) SFS	A5052H32	stabilized	not welded
(2) SFN	A5052H112	unstabilized	not welded
(3) RS	AA6063	unstabilized	not welded
(4) SW	A5052H32	stabilized	shallow welded, v_{weld}=6 m/min
(5) DW	A5052H32	stabilized	deep welded, v_{weld}=2 m/min
(6) BW	A5052H32	stabilized	butt- welded, v_{weld}=2 m/min
(7) GC	A5052H32	stabilized	graphite coated, v_{weld}=2.5 m/min

v_{weld} denotes the welding speed. SW, DW and GC are welded by the bead-on-plate method.

3.2 Dynamic characteristics of WB and first WB

For diagnosis of the deformation status, we note two factors: the dynamic characteristics of the WB and the appearance of the first WB. The former indicates if strain localization is intensive and the latter indicates when the meso-level strain localization is initiated.

The WBs observed in this investigation can be generally classified into three types in terms of the dynamic characteristics: (i) first-moving-eventually-stationary type (called move-and-stay, MS type), (ii) stationary-from-the-beginning type (called stay-and-stay, SS type), (iii) start-appearing-at-a-late-stage-and-directly-stationary type (called late-start-stationary, LS type). From these characteristics of the WB we can diagnose the stress condition of a sample, as discussed below.

3.3 SFN and SFS

These are the samples that we did not weld and therefore assumed to be free of initial stress concentration. Fig.5 and 6 show the dynamic characteristics of the WB and the corresponding stress-strain characteristics for these samples. The dynamic characteristics are expressed by the WB location in the pixel number whereas the stress-strain characteristics are expressed by the tensile load in kN. Both are plotted as a function of object elongation in mm. Points A, B and C indicated in Fig.5 denote, respectively, the point when the first WB appears, the WB starts decelerating, and the WB becomes completely stationary. Point F denotes the vertical location where the fracture occurs. Apparently, SFS shows an MS type WB and SFN shows an SS type WB. Note in Fig.5 that the moment the first WB appears coincides with the initiation of the zigzag character of the stress-strain curve. This indicates that, as mentioned above (see 2.2), the movement of a plastic deformation carrier is responsible for the formation of a WB. The fact that the stress keeps relaxing and increasing reciprocally indicates that the strain localization represented by one WB fades out before the next strain localization represented by another WB is generated. Thus it is most likely that each of the MS type WBs corresponds to different stress concentration. In the case of Fig.6, on the other hand, the stress does not show the zigzag characteristics, indicating that in this case a single stress concentration is responsible for the fracture.

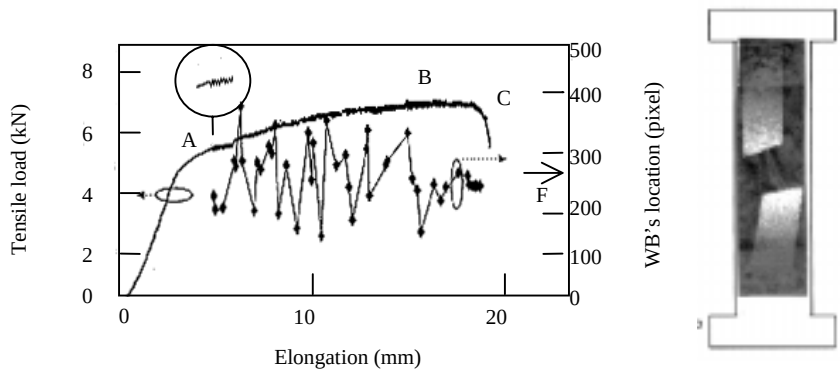

Fig.5 Dynamic characteristics of WB observed in SFS. The image at the right shows the fracture.

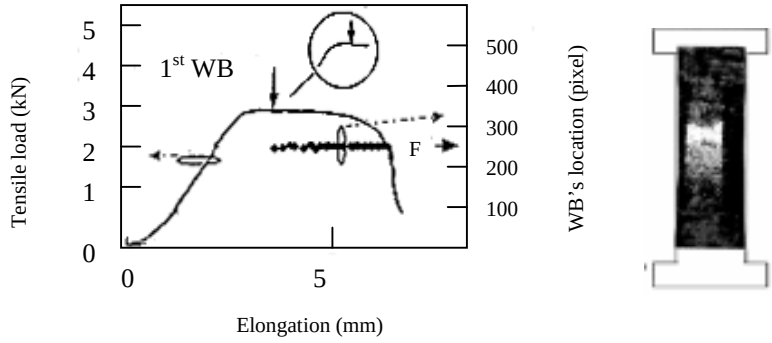

Fig.6 Dynamic characteristics of WB observed in SFN. The image at the right shows the stationary WB.

While the dynamic characteristics of the WB are completely different, SFS and SFN have important properties in common. First and most importantly, both specimens fracture at

the location where the WB becomes stationary. (Note that the pixel number where the WB becomes stationary in the dynamic characteristics in Fig.5 is the same as where the fracture is seen in the object image shown right to the dynamic characteristics. In Fig.6, the fracture occurred at the stationary WB location, though an image of the fractured object is not shown.) Second, the first WB appears as soon as the object enters the plastic region in the stress-strain characteristics. Third, once the WB becomes completely stationary (point C in Fig.5), the stress begins to decrease. These can be interpreted as follows. First, from the fact that the sample fractures at the location of a stationary WB indicates that apparently the intensive strain localization manifested as the stationary WB causes the fracture. Second, the fact that the first WB appears after the material enters into plastic region indicates that in both cases the sample initially does not have stress concentration in the level to causes local plasticity in a particular part of the object before it yields globally. In other words, it is only after the whole sample shows global plasticity that the part of the object reaches the deformation-level in which the stress concentration is high enough to cause a mesoband observed as a WB. The third observation that the stress begins to decrease as soon as the WB becomes stationary indicates that once the deformation reaches the level of intensive strain localization its further evolution is rather uniform over the whole sample. This is contrastive to the situation where a part of the material has an intensive initial stress concentration. In such a case the sample can be work hardened even after a stationary WB appears at a certain location. (see below).

Based on this interpretation, the behavior of the respective samples can be explained as follows. Since the two samples are the same in the material compositions and the post casting hardening treatment, and the only difference is that SFS is stabilized after the hardening treatment, the difference in the dynamic characteristics of WB is considered to be caused by whether or not this stabilization treatment is given. In the case of SFN, when the first WB appears around the yield point the strain localization is already on the level of a stationary WB due to the post casting hardening treatment not followed by stabilization treatment. At the location of the stationary WB, there should initially be stress concentration that is larger in scale than other locations so that the stress relaxes by further developing deformation at this particular location, but not large enough to be manifested as a WB. In the case of SFS, on the other hand, the stabilization treatment homogenizes stress concentration so that there is no particular region that has higher stress concentration than the other parts and this causes the WB to be dynamic until a late stage. Thus from the dynamic characteristics of the WB, we can diagnose that a sample, which we did not weld and therefore believed to be free of initial stress concentration, had actually a low level stress concentration from the beginning.

3.4 RS

The peculiarity of the RS sample is that it shows different WB types among different samples cut from the same bulk material. This is probably because as a low grade material, it lacks homogeneity in the mechanical property. Thus, while SFS and SFN show only one WB type, namely MS type and SS type WB, respectively, RS shows all of MS, SS and LS type WBs depending on the mechanical property possessed by that particular part of the bulk material. Interestingly, this diversity provides us with an insight into the relationship between the WB type and global plasticity.

In Table2, we summarize the types of the WB that we observed in fifteen samples prepared from the same RS bulk material. For each sample, we show the maximum load (the tensile load when the object is under the ultimate tensile strength) and parameters representing where the first WB, the yield point, the first stationary WB, maximum load, fracture are found on the stress-strain characteristics. These parameters are expressed in the unit of the serial data acquisition number. From Table2 the following features are found.

(i) In the cases of MS type and SS type, the first WB is observed near the yield point, as is the case of samples SFS and SFN.
(ii) For all types of WB, once a WB becomes stationary, soon or later the stress begins to decrease. (Compare the first stationary WB point and the maximum load point. They are close to each other regardless of the type of the WB.) This is also consistent with the case of SFS and SFN.
(iii) The MS type and SS type tend to show lower maximum loads and longer distances between the yield point and fracture point than the LS type. This means that the MS type and SS type are lower in the ultimate tensile strength and higher in ductility. In other words, it seems that the earlier the first WB appears, the more plastic the object is. Thus we introduce another parameter called plastic factor defined as (yield point - fracture point)/maximum load, where yield point and fracture point are in data number, and examine its relationship with the appearance of the first WB point. Note that the numerator of the plastic factor indicates the length of the plastic region in the stress-strain characteristics while the denominator indicates the ultimate tensile strength. Fig.7 shows the plastic factor and the maximum load as a function of the first WB point (the data acquisition number where the first WB is observed). It is certainly seen that the earlier the WB starts appearing, the lower is the maximum load and the higher is the plastic factor. This is understandable because earlier appearance of a WB means a faster growth rate of defects, hence faster evolution of plastic deformation.

Table 2. Summary of RS

WB type	1st WB (data#)	max load (kN)	yield point (data#)	1st stationary WB point (data#)	max load point (data#)	fracture point (data#)	plastic factor
MS	50	4.48	60	180	175	195	30.1
MS	44	4.08	44	150	150	171	31.1
LS	143	6.14	101	143	151	161	9.8
LS	98	6.07	49	98	105	116	11.0
LS	138	6.62	63	138	142	156	14.0
LS	122	5.8	81	122	131	146	11.2
MS	50	5.8	50	157	156	184	23.1
LS	107	6.9	61	107	111	126	9.42
MS	15	4.0	16	95	124	146	32.5
LS	72	5.0	28	72	93	106	15.6
LS	94	6.0	29	94	100	116	14.5
LS	121	7.0	39	121	123	141	14.6
LS	96	7.0	45	96	109	126	11.6
LS	100	6.3	30	100	103	121	14.4
SS	31	3.7	30	31	31	104	20

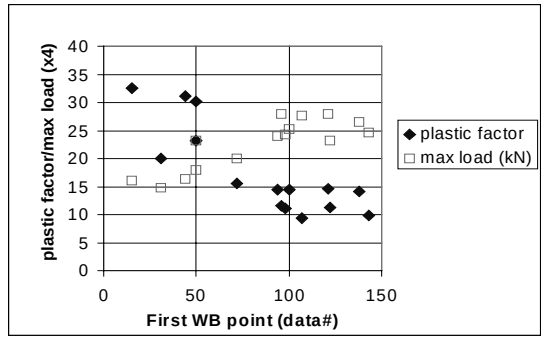

Fig.7 Plastic factor and maximum load.

3.5 Sample with welds

Figs 8 - 11 show the dynamics characteristics and stress-strain curves for the welded samples together with a WB observed in the final stage. The material for these samples is the same as SFS. When a sample is welded, voids formed in the heat-affected zone around the weld cause stress concentration. Defect densities for these samples are shown in Fig.12**.** Below we discuss the dynamic characteristics of WB observed in the respective samples.

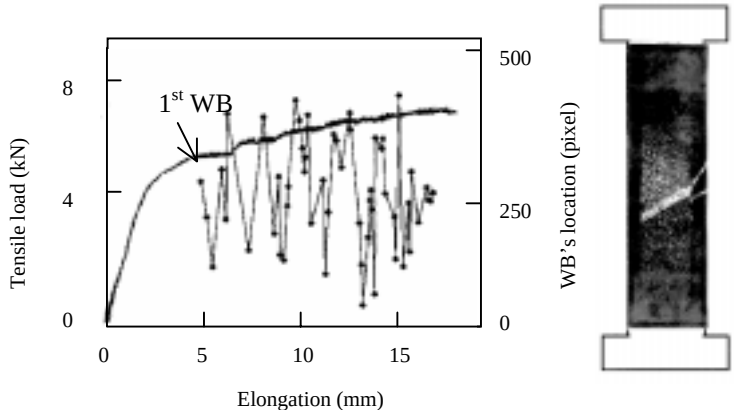

Fig.8 WB observed in shallow-welded (SW) sample.

The WB observed in the SW sample in which the void density is very low shows basically the same dynamic characteristics as the non-weld case (SFS). The WB begins to appear past the yield point and it is dynamic until a very late stage. This indicates that the initial stress concentration is negligibly small. Note that however, the sample eventually fractures along the welded line. From this standpoint, the initial stress concentration caused by weld influences the fracture, while its degree is not higher enough than the other part of the material to cause a stationary WB.

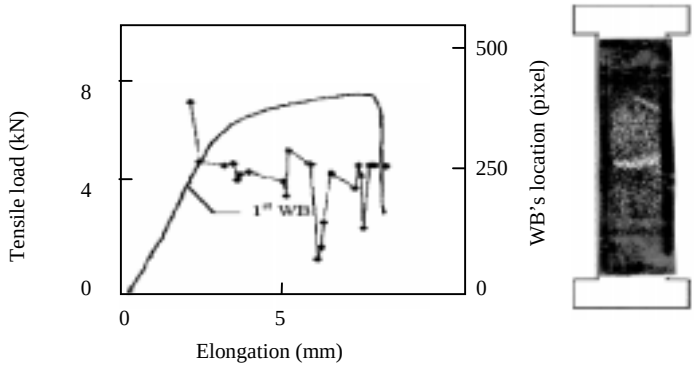

Fig.9 WB observed in deep-welded (DW) sample.

When the sample is deep-welded (DW), the first WB appears before the yield point. This indicates that there is local plasticity that causes strain localization manifested as a WB in the stage of deformation when other parts can still be work hardened. The dynamic

characteristics of the WB is basically stationary but occasionally dynamic. This is a sort of intermediate between the cases of the shallow-welded sample and the butt-welded sample. It is interesting that unlike the non-weld and shallow-welded cases, the stress-strain curve does not show zigzag characteristics. This indicates that in the case of the DW sample, the stress relaxation is actualized by enhancing the strain localized at this pseudo-stationary WB rather than by generating abrupt stress decrease being associated with WB occasionally observed at other locations. Note that as soon as the WB finally gets stationary, the stress decreases as is the non-welded case.

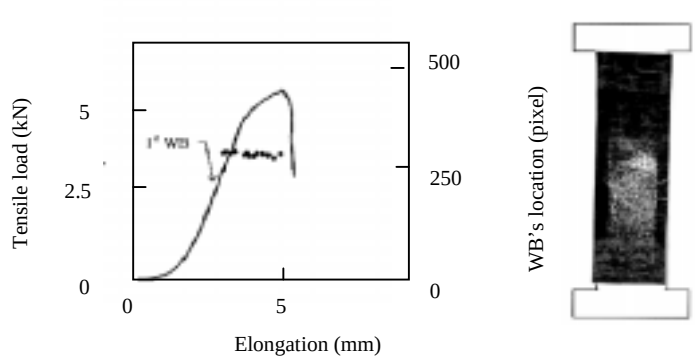

Fig.10 WB observed in butt-welded (BW) sample.

In the case of the butt-welding (BW), the WB is completely stationary from the beginning at the weld where the sample fractures. The first WB is observed in the elastic region of the stress-strain curve. It can be said that the initial stress concentration of this sample is strong enough to cause intensive strain localization at the weld and maintain it at the same location until the material fractures. As is the case of the deep welding, after the appearance of the first WB the other part of the sample is still work hardened. This indicates that the level of the local plasticity of the butt-welded sample is such that the associated strain localization is intensive enough to make the WB stationary but since it is localized the other part of the material can be work hardened.

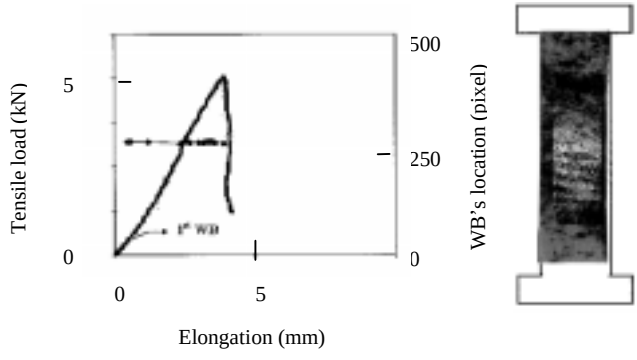

Fig.11 WB observed in graphite-coated (GC) sample.

When the sample is coated by graphite, it is well known that the void density is increased. In this case, the WB begins to appear as soon as the tensile load is started. The WB is stationary from the beginning and the sample fractures before the stress-strain curve

reaches the yield point. The characteristics of the local plasticity is basically similar to the case of the butt-welded sample, but since the associated strain localization is more intensive the first WB appears earlier and the material fractures there while other part is still being work hardened. In other words, the level of local plasticity is higher than the BW sample and it can cause the sample to fracture while the other part is still being work hardened.

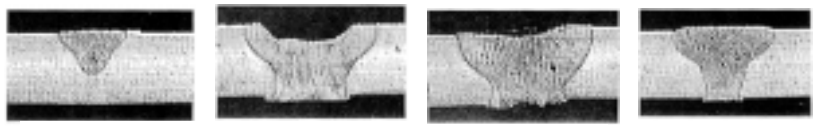

Fig.12 Voids observed around weld. Voids are seen as black dots.

Table 3. Summary of welded samples

weld type	void density	1st WB region	WB type	Max load (kN)	yield load (kN)	stationary WB location (pixel#)	fracture location (pixel #)
no weld	no	plastic	MS	9.2	6.5	296/274*	296/274*
Shallow	no	plastic	MS	6.5	4	236/272*	236/272*
Deep	very low	elastic	MS	7.6	6.8	264	264
Butt	low	elastic	SS	4.5	3.6	240	240
Graphite	high	elastic	SS	5.0	-	252	252

Samples are welded at the center of the sample (pixel#240 - 260)
* Two numbers denote the right and left locations of the WB/fracture line.

Table 3 summarizes the results of welded samples. Note that in all the cases the sample fractures at the location where the WB becomes stationary.
From these observations, the following things can be said:
(1) All the samples eventually fracture where WB becomes stationary
(2) WB becomes stationary at the weld
(3) As the void density, hence the degree of initial stress concentration, increases, the WB tends to (i) begins to appear earlier than the yield point and (ii) tends to be stationary from the beginning.

In (3), (i) indicates local plasticity and (ii) indicates that the level of associated strain localization is intensive from the beginning. In terms of the level of the initial stress concentration, (i) can appear at a lower level. In other words, when the degree of the initial stress concentration increases, the first symptom is the initiation of local plasticity that is manifested as the first WB appearing in the elastic region. As the level of the initial stress concentration increases, the local plasticity can cause intensive strain localization manifested as a WB stationary from the beginning. In this fashion, it is possible to diagnose the level of the initial stress concentration by noting when the first WB appears and whether it is stationary.

4. Summary

In conclusion, the series of experiment show that the WB represents strain localization and its characteristics are well explained by mesomechanics. From what described above, the overall criteria of diagnosis of the material's mechanical condition based on the observation of the WB can be summarized as follows.

(1) The WB appears when meso-scale strain localization is initiated in the material.
(2) When the degree of the strain localization has not reached the intensive level, the WB is dynamic. While the WB is dynamic, the material does not fracture.
(3) When the degree of the strain localization has reached the intensive level, the WB becomes stationary and the material can fracture at that location at any moment.
(4) If the material is free of initial stress concentration, the first WB appears after the yield point (in the plastic region).
(5) When the material has initial stress concentration, the first WB can appear in the elastic region and the degree of the initial stress concentration can be diagnosed as follows.

(5.1) If the degree of the initial stress concentration is not high enough to cause intensive strain localization, the WB is dynamic.

(5.2) If the degree of the initial stress concentration is high enough to cause strain localization, the WB appearing in the elastic region can be stationary from the very beginning.

Acknowledgments

This work was partly supported by Japan Science and Technology Corporation. The welded samples were prepared at the Institute of Research and Innovation. We are grateful to all the students who supported the experiment. Helpful discussion and advice by Prof. Satoru Toyooka is highly appreciated. We thank Alexandre Gorlenko for his support in image data processing.